



Deposited via The University of Sheffield.

White Rose Research Online URL for this paper:

<https://eprints.whiterose.ac.uk/id/eprint/132819/>

Version: Accepted Version

Article:

Rubinato, M., Lee, S., Martins, R. et al. (2018) Surface to sewer flow exchange through circular inlets during urban flood conditions. *Journal of Hydroinformatics*, 20 (3). pp. 564-576. ISSN: 1464-7141

<https://doi.org/10.2166/hydro.2018.127>

Reuse

Items deposited in White Rose Research Online are protected by copyright, with all rights reserved unless indicated otherwise. They may be downloaded and/or printed for private study, or other acts as permitted by national copyright laws. The publisher or other rights holders may allow further reproduction and re-use of the full text version. This is indicated by the licence information on the White Rose Research Online record for the item.

Takedown

If you consider content in White Rose Research Online to be in breach of UK law, please notify us by emailing eprints@whiterose.ac.uk including the URL of the record and the reason for the withdrawal request.

1 **Surface to sewer flow exchange through circular inlets during urban**
2 **flood conditions**

3 Matteo Rubinato, Seungsoo Lee, Ricardo Martins and James D.
4 Shucksmith

5 **Matteo Rubinato**

6 **Ricardo Martins**

7 **James D. Shucksmith**

8 The University of Sheffield, Civil and Structural Engineering Department, Sir Frederick
9 Mappin Building, Mappin Street, S1 3JD, Sheffield, UK

10 **Seungsoo Lee** (corresponding author)

11 APEC Climate Center, 12 Centum 7-ro, Haeundae-gu, Busan, 612-020, Republic of
12 Korea, 48058

13 E-mail: seungsoo_lee@apcc21.org

14 **Ricardo Martins**

15 MARE - Marine and Environmental Sciences Centre, Department of Civil Engineering,
16 FCT, University of Coimbra, Coimbra, Portugal

17 **Ricardo Martins**

18 IMAR - Institute of Marine Research, FCT, University of Coimbra, Coimbra, Portugal

19

20 **ABSTRACT**

21 Accurately quantifying the capacity of sewer inlets (such as manhole lids and
22 gullies) to transfer water is important for many hydraulic flood modelling tools.

23 The large range of inlet types and grate designs used in practice makes the
24 representation of flow through and around such inlets challenging. This study uses
25 a physical scale model to quantify flow conditions through a circular inlet during
26 shallow steady state surface flow conditions. Ten different inlet grate designs have

27 been tested over a range of surface flow depths. The resulting datasets have been
28 used (i) to quantify weir and orifice discharge coefficients for commonly used
29 flood modelling surface–sewer linking equations; (ii) to validate a 2D finite
30 difference model in terms of simulated water depths around the inlet. Calibrated
31 weir and orifice coefficients were observed to be in the range 0.115–0.372 and
32 0.349–2.038, respectively, and a relationship with grate geometrical parameters
33 was observed. The results show an agreement between experimentally observed
34 and numerically modelled flow depths but with larger discrepancies at higher flow
35 exchange rates. Despite some discrepancies, the results provide improved
36 confidence regarding the reliability of the numerical method to model surface to
37 sewer flow under steady state hydraulic conditions.

38 **Key words** | experimental modelling, numerical modelling, surface to
39 sewer flow exchange, urban flooding, discharge coefficients

40 **INTRODUCTION**

41 Current climatic trends mean that the frequency and magnitude of urban
42 flooding events is forecast to increase in the future (Hammond *et al.* 2015) leading to
43 increased damage in terms of loss of business, livelihoods plus increased inconvenience
44 for citizens (Ten Veldhuis & Clemens 2010). These potential impacts underline the
45 importance of accurate modelling tools to determine flow paths within and between
46 overland surfaces and sewer/drainage systems. Existing urban flood models commonly
47 utilise the 1D Saint-Venant and 2D Shallow Water Equations (SWE) to calculate flows
48 within sewer pipes and on the surface (overland flow) (Martins *et al.* 2017b). However,
49 modelers are also faced with the concern of how to correctly reproduce the hydraulic
50 behaviour around and within complex and variable hydraulic structures such as
51 manholes and gullies which are used to connect the surface system to the sewer system.
52 Unless the inlet is blocked or the sewer is surcharged, these structures allow water to be
53 drained from the surface. An inaccurate representation of inlet capacity can lead to
54 incorrect prediction of flow volumes, velocities and depths on the surface (Xia *et al.*
55 2017), as well as in the sewer pipes. Due to their geometrical complexity such linking
56 structures are conventionally represented using weir and orifice equations within urban
57 flood models (Djordjevic' *et al.* 2005; Chen *et al.* 2007; Leandro *et al.* 2009; Martins *et*

58 *al.* 2017a). However, due to a paucity of datasets, the robust calibration and validation
59 of such linking methodologies is lacking. In particular, the determination of appropriate
60 discharge coefficients for such linking equations over a range of hydraulic conditions
61 and inlet types is required. Experimental studies investigating surface–sewer flow
62 interaction via gullies and manholes are scarce (Martins *et al.* 2014). Larson (1947)
63 identified inlet width and the efficiency of the inlet opening as characteristics of
64 primary importance to determine inlet capacity; Li *et al.* (1951, 1954) experimentally
65 investigated the effectiveness of some grate inlets in transferring flow from surface to
66 sewer by treating the flow bypassing the grate as separate portions, and Guo (2000a,
67 2000b) and Almedej & Houghtalen (2003), proposed different modifications to grate
68 inlet design. Gómez & Russo (2009) investigated the hydraulic efficiency of transverse
69 grates within gully systems proposing new mathematical expressions to define the
70 hydraulic efficiency. Gómez & Russo (2011a) studied the hydraulic behaviour of inlet
71 grates in urban catchments during storm events and Gómez *et al.* (2011b) presented an
72 empirical relationship to obtain the hydraulic efficiency as a function of inlet and street
73 flow characteristics. In further work, Gómez *et al.* (2013) investigated the hydraulic
74 efficiency reduction as a result of partially clogged grate inlets. More recently, Rubinato
75 *et al.* (2017a) experimentally validated the ability of weir/orifice linking equations to
76 represent steady flow exchange through a scaled open manhole. However, the
77 performance was dependent on the calibration of the discharge coefficients as well as a
78 robust characterisation of the flow within the sewer and flow depth on the surface such
79 that the hydraulic head difference between surface and sewer flows could be accurately
80 determined. An accurate representation of flow exchange is therefore also dependent on
81 correctly modelling of flow conditions (hydraulic head) in the vicinity of the inlet
82 structure. Literature published to date lacks repeatable tests of different grate inlets
83 under controlled conditions and an integration of results into modelling tools.
84 Numerical studies of flows around gullies and manholes are limited due to a lack of
85 experimental data as well as long computational times when simulating complex 3D
86 flows (Leandro *et al.* 2014). However, some studies have been conducted: Lopes *et al.*
87 (2015) analysed experimental results from a surcharging jet arising from the reverse
88 flow out of a manhole after the sewer system became pressurised; Djordjevic' *et al.*
89 (2013) focused on surface recirculation zones formed downstream of gullies; both
90 studies have used experimental data to model flow patterns inside gullies and manholes
91 using CFD; Rubinato *et al.* (2016) studied flow depths around an open circular manhole

92 under drainage conditions and validated a 2D finite difference model. Martins *et al.*
93 (2017a) validated two finite volume (FV) flood models in the case where horizontal
94 floodplain flow is affected by sewer surcharge flow via a manhole demonstrating that
95 the shock capturing FV-based flood models are applicable tools to model localised
96 sewer-to-floodplain flow interaction. However, no studies to date have looked
97 specifically at the influence of different grate cover designs/geometries on flow
98 exchange capacity, flow conditions around the inlet and the ability of 2D modelling
99 tools to replicate depths around the inlet over a range of flows. The objective of this
100 work is to use a physical scale model to collect an extensive series of experimental
101 datasets describing surface to sewer flow exchange through a circular inlet under steady
102 state conditions through ten different inlet grate configurations. The datasets are used to
103 (i) determine appropriate weir/orifice discharge coefficients applicable to describe
104 exchange flows and (ii) to validate the ability of a calibrated 2D numerical finite
105 difference method (FDM) to describe observed surface flow depths in the vicinity of the
106 inlet structure.

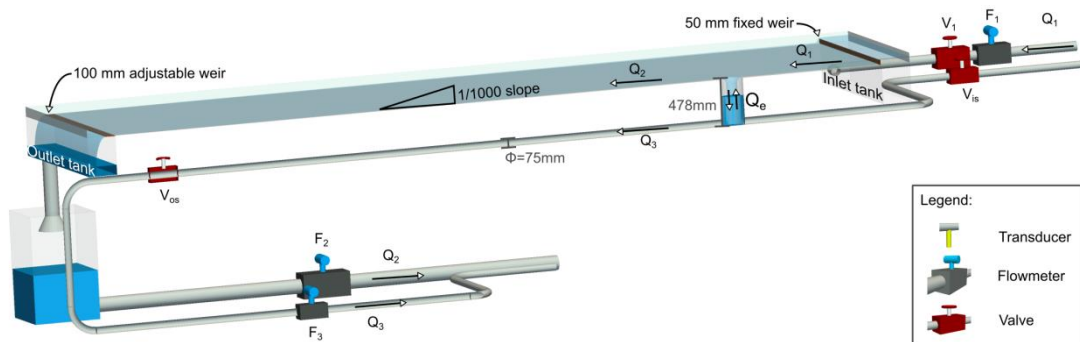
107 **METHODOLOGY**

108 This section presents (i) the experimental facility used to collect the data, (ii) hydraulic
109 conditions for the tests conducted, (iii) a detailed procedure of the methods used to
110 estimate discharge coefficients of the linking equations and (iv) a description of the
111 numerical flood model utilised.

112 **Experimental model**

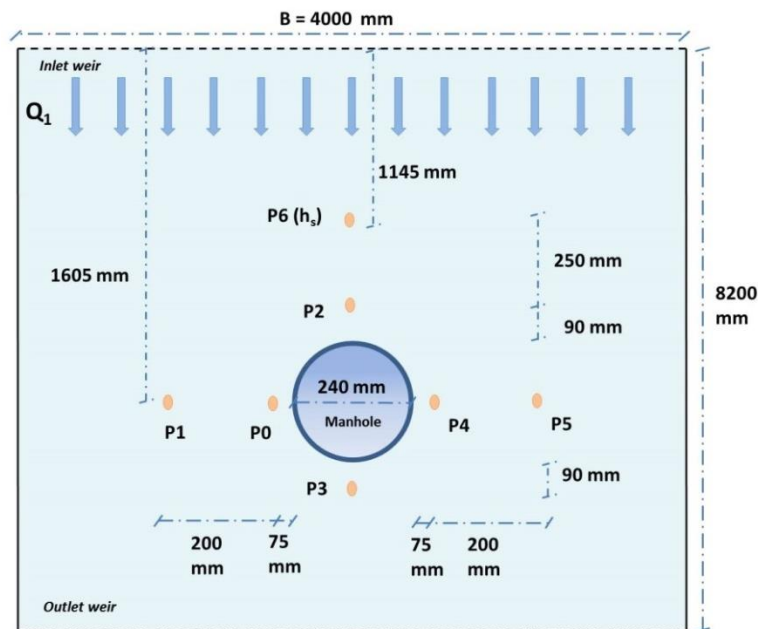
113 The experimental set-up utilised (Figure 1) was assembled at the water laboratory of the
114 University of Sheffield (UK) (Rubinato 2015). It consists of a scaled model of an urban
115 drainage system/floodplain linked via a manhole shaft. The floodplain surface (4 m,
116 width, by 8.2 m, length) has a longitudinal slope of 1/1000. The urban drainage system
117 is made from horizontal acrylic pipes directly beneath the surface (inner diameter =
118 0.075 m). One circular acrylic shaft (representing a manhole) with 0.240 m inner
119 diameter and 0.478 m height connects the surface to the pipes. The facility is equipped
120 with a SCADA system (Supervision, Control and Data Acquisition) through Labview™
121 software that permits the setup and monitoring of flow rates within the surface and
122 sewer systems independently. A pumping system in a closed circuit supplies water

123 within the facility. The inlet pipes (V_1 , V_{is}) are fitted with electronic control valves
 124 operated via Labview™ software. The surface downstream outlet is a free outfall which
 125 contains an adjustable height weir.



126

127 **Figure 1** | Scheme of the experimental facility (Rubinato *et al.* 2017b).



128

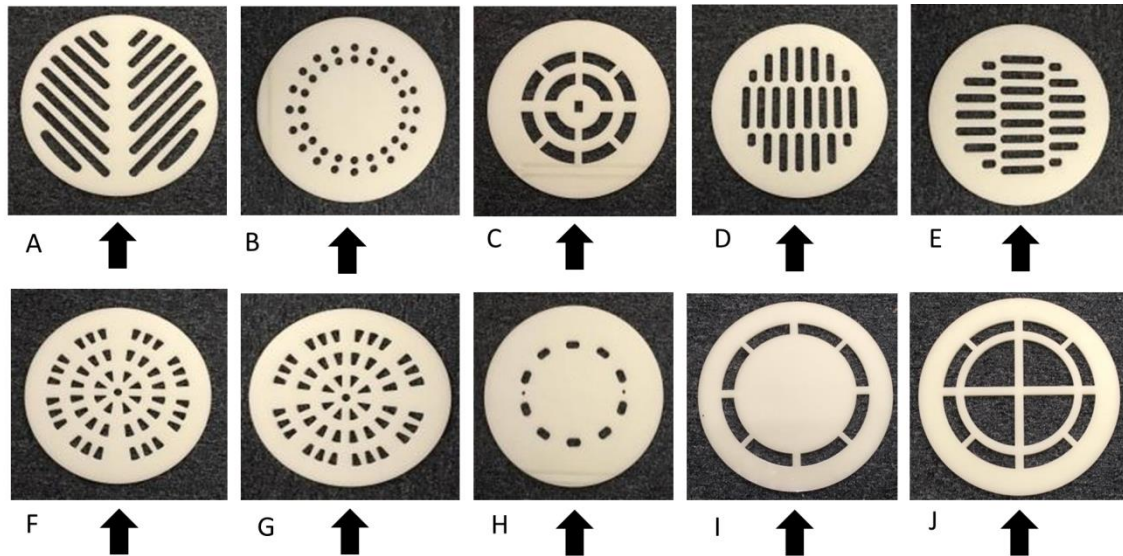
129 **Figure 2** | Location of the pressure transducer measurement points around the surface to
 130 sewer drainage inlet (not to scale).

131 Calibrated electro-magnetic (MAG) flow meters (F_1 , inlet floodplain; F_2 , outlet
 132 floodplain; F_3 outlet sewer) were installed in the upstream and downstream pipes in
 133 order to measure the surface system inflow (Q_1) and surface and sewer outflows (Q_2 ,
 134 Q_3) and calculate the steady state drainage rate through the surface to sewer inlet (Q_e).
 135 Each flow meter was independently verified against a laboratory measurement tank. For
 136 the tests reported here, the sewer inflow was not used (sewer inflow = 0) and all flow

137 therefore entered the facility via the surface inlet weir (Q_1). Drainage flow passed via
 138 the drainage inlet to the sewer outlet ($Q_e = Q_3$), with the remaining flow passing over
 139 the facility to downstream outlet weir (Q_2). Flow depth on the floodplain was measured
 140 by a series of pressure sensors (of type GEMS series 5000) fitted at various locations
 141 around the inlet (Figure 2) (with an accuracy of ± 0.109 mm for the range of water depth
 142 0–100 mm). Ten different grate types were constructed from acrylic using a laser cutter
 143 and installed within the drainage structure and tested under steady state conditions in
 144 order to obtain flow depth vs drainage discharge (Q_e) relationships for each grate type.
 145 The grate opening types were selected based on common types used in different
 146 countries, and are presented in Figure 3. For each grate opening type the total area of
 147 empty space (A_e) and total effective edge perimeter length (P_v) were obtained from the
 148 AutoCAD drawings prior to fabrication (Table 1). Autocad drawings are included as
 149 supplementary data.

150 **Table 1** | Technical details of the grids utilised

Grate	Area filled A_f (m^2)	Area empty spaces A_e (m^2)	Void ratio V (%)	Effective perimeter P_v (m)
A	0.0307	0.0145	32.1	3.0364
B	0.0421	0.0031	6.9	1.2520
C	0.0373	0.0079	17.48	1.3880
D	0.0353	0.0099	21.9	2.3794
E	0.0353	0.0099	21.9	2.3794
F	0.0391	0.0061	13.5	2.2586
G	0.0391	0.0061	13.5	2.2586
H	0.0435	0.0017	3.76	0.5128
I	0.0385	0.0067	14.11	1.2428
J	0.0277	0.0175	38.03	1.8816



152

153

154

Figure 3 | Grates applied on the top of the inlet (black arrows show the primary direction of the facility inflow Q_1 and hence the orientation of each inlet grate).

155

Hydraulic conditions

156

157

158

159

160

161

162

163

164

165

166

167

168

169

170

171

For each grate inlet displayed in Figure 3, eight tests have been completed over a range of surface inflows (Q_1) between 4 and 10 l/s set using the upstream valve (V_1). This is equivalent to a unit width discharge ($q_1 = Q_1/B$) between 1 and 2.5 l/s. To ensure reliable depth and flow rate quantification for each test, flows were left to stabilise for 5 minutes before flow rates and depths were recorded. Each reported depth/flow measurement is a temporal average of 3 minutes of recorded data after flow stabilisation, such that full convergence of measured parameters is achieved. In all cases, a flat weir was used as the downstream floodplain boundary, and free surface flow was maintained in the pipe system. The upstream flow depth (h_s) is reported as the depth recorded at transducer P_6 (Figure 2). Surface flow Froude number (Fr) is calculated based on this flow depth and the calculated cross-sectional averaged velocity (U) at this position ($U = Q_1/B.h_s$). The hydraulic conditions for each test are detailed in Table 2. Full (non-averaged) datasets from flow meters Q_1 , Q_3 and transducers (P_0 , P_1 , P_2 , P_3 , P_4 , P_5 , P_6) are presented as supplementary data (Table S1) to this paper.

172 **Table 2** | Hydraulic parameters measured (Q_I , Q_e and h_s) and calculated (Fr) for the
 173 tests conducted

Grate	Q_I	Q_e	h_s	Fr	Grate	Q_I	Q_e	h_s	Fr
	(l/s)	(l/s)	(mm)	(/)		(l/s)	(l/s)	(mm)	(/)
A	4.33	0.55	7.28	0.556	B	4.29	0.50	7.26	0.554
	5.00	0.67	7.89	0.569		4.99	0.59	7.92	0.565
	5.66	0.76	8.50	0.576		5.67	0.68	8.60	0.568
	6.32	0.86	9.09	0.582		6.33	0.76	9.15	0.577
	6.93	0.93	9.49	0.599		6.93	0.82	9.63	0.586
	7.51	0.94	10.05	0.595		7.52	0.89	10.12	0.590
	8.22	1.05	10.60	0.601		8.18	0.91	10.64	0.596
	9.29	1.19	11.36	0.612		9.22	0.94	11.42	0.603
C	4.29	0.43	7.53	0.524	D	4.23	0.43	7.72	0.498
	4.97	0.54	8.16	0.539		4.96	0.59	8.40	0.514
	5.66	0.63	8.91	0.538		5.69	0.70	9.24	0.512
	6.32	0.72	9.53	0.542		6.30	0.72	10.11	0.495
	6.95	0.74	10.10	0.546		6.96	0.80	10.72	0.501
	7.54	0.80	10.60	0.552		7.49	0.82	11.18	0.506
	8.21	0.88	11.14	0.558		8.19	0.96	11.70	0.516
	9.28	0.97	11.91	0.570		9.24	1.09	12.49	0.529
E	4.27	0.44	7.36	0.540	F	4.28	0.44	7.40	0.537
	5.00	0.53	8.02	0.555		4.95	0.48	8.07	0.545
	5.68	0.63	8.62	0.566		5.66	0.61	8.75	0.552
	6.31	0.69	9.19	0.572		6.37	0.70	9.40	0.558
	6.96	0.77	9.70	0.582		6.96	0.85	9.74	0.577
	7.51	0.81	10.01	0.582		7.52	0.90	10.20	0.582
	8.19	0.90	10.59	0.600		8.17	0.95	10.63	0.595
	9.24	0.99	11.42	0.605		9.25	1.10	11.49	0.599
G	4.22	0.48	7.60	0.508	H	4.26	0.39	7.25	0.551
	4.93	0.61	8.27	0.523		4.97	0.44	7.96	0.558
	5.63	0.72	9.01	0.525		5.66	0.48	8.68	0.559
	6.26	0.80	9.61	0.530		6.29	0.52	9.35	0.555
	6.87	0.84	10.05	0.544		6.92	0.58	9.82	0.567

	7.52	0.94	10.50	0.558		7.51	0.66	10.30	0.574
	8.21	1.03	11.00	0.568		8.19	0.68	10.77	0.584
	9.22	1.13	11.76	0.578		9.22	0.70	11.57	0.592
I	4.26	0.43	7.28	0.547	J	4.26	0.46	7.44	0.530
	4.97	0.57	7.85	0.571		4.94	0.52	8.13	0.538
	5.64	0.63	8.53	0.571		5.66	0.64	8.78	0.549
	6.27	0.71	9.13	0.573		6.27	0.72	9.39	0.550
	6.92	0.78	9.65	0.583		6.91	0.77	9.87	0.562
	7.51	0.88	10.08	0.593		7.52	0.90	10.35	0.570
	8.16	0.93	10.58	0.599		8.18	0.95	10.84	0.579
	9.22	1.03	11.39	0.605		9.21	0.98	11.66	0.584

174

175 *Discharge coefficients*

176 Within flood modelling applications the weir (1) and orifice (2) equations are
177 commonly defined as the following (Rubinato *et al.* 2017a):

$$178 \quad Q_e = \frac{2}{3} C_w \pi D_m \sqrt{2g} (H)^{\frac{3}{2}} \quad (1)$$

179 where D_m is the diameter of the (circular) inlet (m), H is the driving hydraulic head
180 above the interface point accounting for both sewer and surface flows (m). C_w is the
181 weir discharge coefficient.

$$182 \quad Q_e = C_o A_m \sqrt{2gH} \quad (2)$$

183 where A_m is the open area of the inlet and C_o is the orifice coefficient. In cases
184 where the sewer is not surcharged, the hydraulic head (H) is assumed to be equal to the
185 surface flow depth. To calibrate discharge coefficients for each grate type, Equations (2)
186 and (3) were modified to account for the total length of the weir within each grate
187 design (taken as equal to P_v) and total open area (taken as equal to A_e). The flow depth
188 is taken as the measured upstream value (h_s).

$$189 \quad Q_e = \frac{2}{3} C_w P_v \sqrt{2g} (h_s)^{\frac{3}{2}} \quad (3)$$

$$190 \quad Q_e = C_o A_e \sqrt{2g} (h_s)^{\frac{1}{2}} \quad (4)$$

191 Numerical model

192 The depth-averaged 2D SWEs are commonly used for modelling flows in urban
193 environments and in rivers and floodplains (Wang *et al.* 2011). Integrating an inflow
194 and outflow in/from the sewerage system can be realised by adding suitable source
195 terms (Lee *et al.* 2013). The governing equations used for floodplain modelling with
196 surface to sewer inflows are as follows:

$$197 \quad \frac{\partial h}{\partial t} + \frac{\partial(uh)}{\partial x} + \frac{\partial(vh)}{\partial y} = -q_e \quad (5)$$

$$198 \quad \frac{\partial(uh)}{\partial t} + \frac{\partial(u^2h)}{\partial x} + \frac{\partial(uvh)}{\partial y} = -gh \frac{\partial E}{\partial x} - gn^2 \frac{u\sqrt{u^2 + v^2}}{h^{1/3}} \quad (6)$$

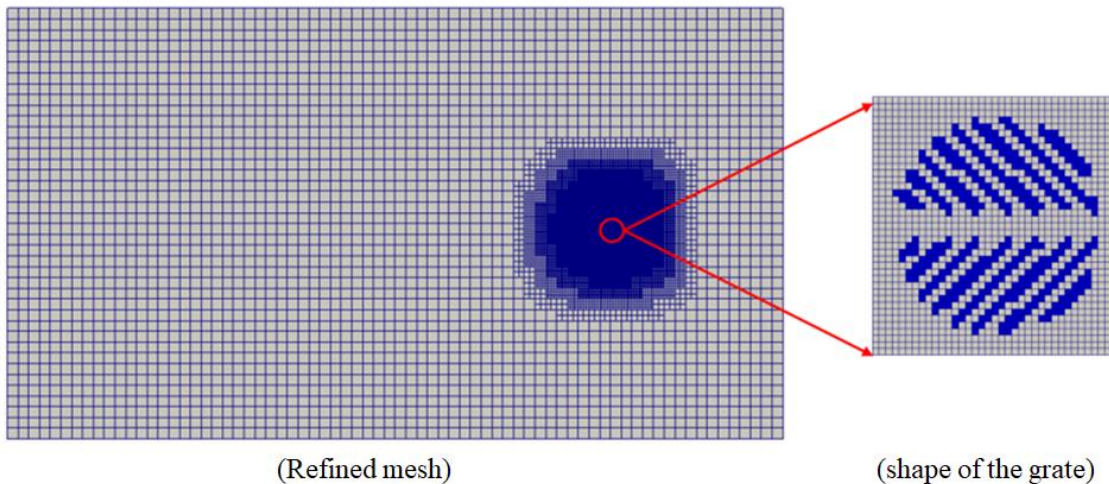
$$199 \quad \frac{\partial(vh)}{\partial t} + \frac{\partial(uvh)}{\partial x} + \frac{\partial(v^2h)}{\partial y} = -gh \frac{\partial E}{\partial y} - gn^2 \frac{v\sqrt{u^2 + v^2}}{h^{1/3}} \quad (7)$$

200 In Equations (5)–(7), (x, y) are the spatial Cartesian coordinates and t is the time (SI
201 units). h (m) is the water depth u and v (m/s) are x- and y-direction velocities,
202 respectively. E is the water elevation (m), and n is Manning’s roughness coefficient
203 (here taken as 0.009 m/s^{1/3}, from previous experimental work, e.g., Rubinato *et al.*
204 (2017a)). q_e (m/s) is the area discharge, in this study representing surface to sewer
205 discharge via the inlet grate. A leap-frog method is used in order to reduce simulation
206 time, with variables laid on staggered mesh. Fluxes (uh and vh) are located at the
207 computational cell boundary and water depth (h) is located at the centre of the
208 computational cell. More detailed information regarding the leap-frog and FDM
209 methods can be found in Lee (2013).

210 Model setup and boundary conditions

211 An adaptive mesh technique (Haleem *et al.* 2015) is used to reduce the calculation time (Figure
212 4). In the simulation, the downstream depth measurement point (P₇) is used to define
213 downstream boundary conditions, hence the initial number of quadrilaterals was chosen to be 72
214 × 40 (7.2 m × 4.0 m) to generate a baseline (coarse) mesh with a spatial resolution of around 0.1
215 m × 0.1 m. A mesh convergence analysis was carried out, which suggested the need for a four
216 times finer mesh for the model to be able to appropriately resolve the hydrodynamics of the
217 grate inlet. As shown in Figure 4, up to four levels of refinement are implemented around the
218 local zone of sewer-to-floodplain interaction (resolution around 6.25 mm × 6.25 mm) and these
219 are assumed appropriate to replicate the geometry of each grate type. The open cells within each

220 grate area are identified as cells where the q_e term in Equation (5) is nonzero. The total flow
221 exchange from surface to sewer is calculated by applying Equation (3) using the experimentally
222 obtained weir coefficients and simulated upstream water depth at P_6 (h_s). q_e for each open cell is
223 then calculated based on the total calculated flow exchange and the total open area of each grate
224 type. All the simulations were run until convergence to a steady state is attained. A mesh
225 convergence analysis suggested the use of a convergence (depth) threshold-error no bigger than
226 10^4 and no less than 10^6 . The initial discharge condition is taken to be the unit width surface
227 inflow q_1 and a measured velocity profile is used to set water depth at the eastern (upstream)
228 boundary. This velocity curve was obtained prior to the experiments by measuring ten flows
229 (Q_1) between 2 l/s and 11 l/s and recording the average velocity in the area included between
230 0.5 and 3.5 m of the total width, with sampling points each 0.5 m. At the southern and northern
231 boundaries (lateral), a wall boundary condition is employed (reflective). At the western
232 (downstream) boundary, measured water depth at P_7 is used.



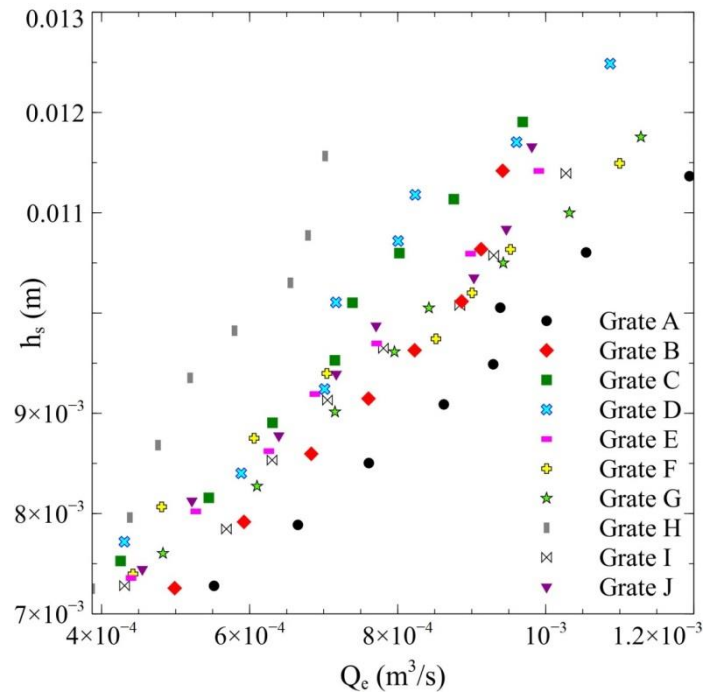
233
234 **Figure 4** | Mesh characterisation example for grate type A.

235 **RESULTS AND DISCUSSIONS**

236 This section presents discharge coefficients estimated for each grate configuration and
237 the comparison of the 2D finite difference model predictions against observed flow
238 depths recorded around the inlet at seven different pressure sensor locations (P_0 – P_6)
239 displayed in Figure 2.

240 **Experimental results and calibrated discharge coefficients**

241 Figure 5 shows the relationship between the upstream water depth (h_s) and the
242 correspondent flow exchange (Q_e) through each grate type over the range of flow
243 conditions tested.



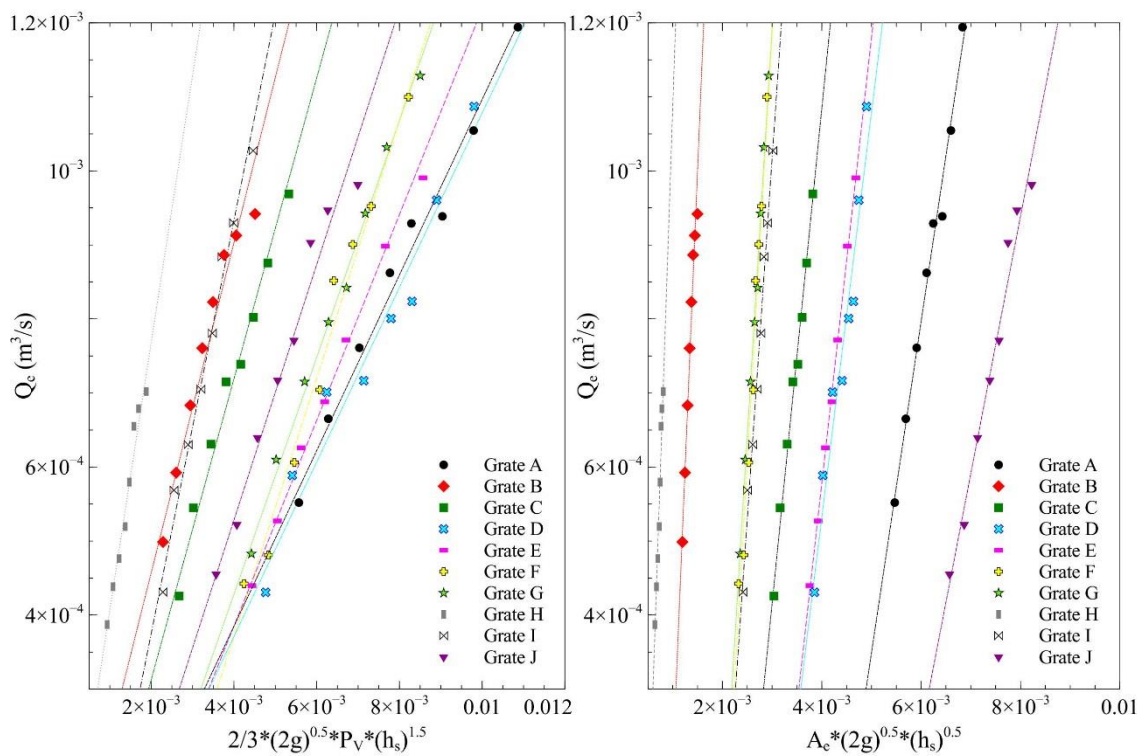
244

245 **Figure 5** | The observed relationship between upstream water depth vs surface to sewer
246 flow exchange for each grate type.

247 The results confirm that the geometry of each grate strongly influences the flow
248 entering the surface-sewer inlet. When comparing results for similar hydraulic
249 conditions, grate H ($A_e = 0.0017 \text{ m}^2$; $P_v = 0.5128 \text{ m}$) is the grate that results in the
250 lowest exchange flows while grate A allows the highest exchange flows ($A_e = 0.0145$
251 m^2 ; $P_v = 3.0364 \text{ m}$). It can be noted that while grate A has the highest perimeter values,
252 its void area is lower than grate J. In general, the results confirm that the exchange flow
253 capacity of each grate design is more strongly correlated to the effective perimeter than
254 the void area; however, individual different grate designs can affect the flow patterns
255 around the void spaces and hence drainage efficiency. To provide a better understanding
256 of this a further investigation including consideration of the local flow velocity is
257 required.

258 Calibration of Equations (3) and (4) is achieved by fitting a linear trend between the
259 terms of the relevant equation and the surface to sewer exchange flow (Q_e) for each
260 grate type (shown in Figure 6). The average goodness of fit of the linkage equations

261 over all grate types (weir equation average $R^2 = 0.977$, orifice equation $R^2 = 0.980$)
 262 shows that both weir and orifice equations are shown to be applicable for representation
 263 of surface to sewer flow exchange in steady flow (confirming previous work, Rubinato
 264 *et al.* (2017a)) and that over the range of hydraulic conditions tested here, the weir and
 265 orifice coefficients can be taken as constant. Calibrating the weir Equation (3) against
 266 the experimental results provides a discharge coefficient C_w in the range 0.115–0.372
 267 based on the variety of grates applied (Table 1). Calibration of the orifice Equation (4)
 268 against the experimental results provides a discharge coefficient C_o in the range 0.349–
 269 2.038. Values for each grate type are provided in Table 3, along with correspondent
 270 goodness of fit values (R^2). Discharge coefficients observed in this study are in the same
 271 range to those found by Martins *et al.* (2014) for a $0.6 \times 0.3 \times 0.3$ m gully under
 272 drainage conditions ($0.16 < C_w < 1.00$, $1.36 < C_o < 2.68$) but differs to those obtained by
 273 Bazin *et al.* (2014) for small (0.05×0.05 m) fully open street inlets ($0.58 < C_o < 0.67$).
 274 This is likely due to the variation in scales between the experimental facilities used. It is
 275 noticeable that the orifice equation results in a larger variation in the range of calibrated
 276 coefficients than the weir equation.

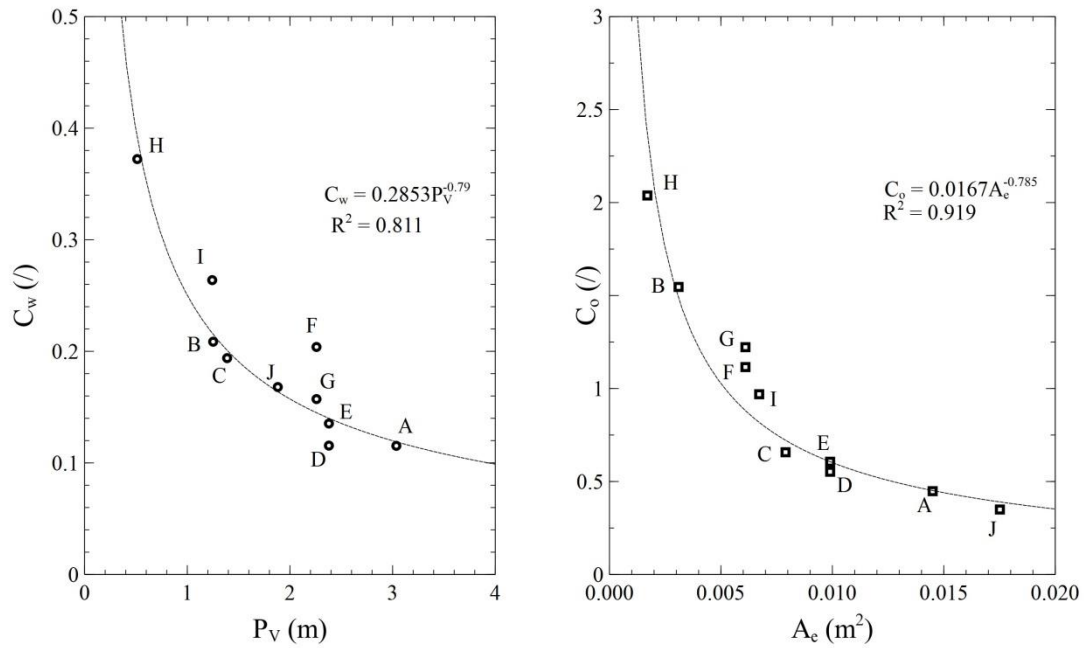


278 **Figure 6** | (left) The relationship between the weir equation (3) for each flow condition
 279 tested vs the correspondent flow exchange; (right) the relationship between the orifice
 280 equation (4) vs the correspondent flow exchange.

281 Calibrated discharge coefficients show an inverse trend with the geometrical parameters
 282 (P_v or A_e) associated with the different grate types, suggesting a higher energy loss
 283 associated with surface to sewer flow transfer as opening size decreases (Figure 7).
 284 Figure 7 shows that coefficients approach an approximately constant value ($C_w \approx 0.115$,
 285 $C_o \approx 0.35$ in this case) as opening size and size and perimeter length increases. The
 286 consideration of individual grate types shows that the application of the weir equation
 287 tends to provide higher R^2 values for grate types when the perimeter length value (P_v) is
 288 relatively large (e.g., grate types D and G), while the orifice equation tends to provides
 289 higher R^2 values for grate types when the perimeter length value is smaller (e.g., grate
 290 types B and C). This may be due to the increased likelihood of grates with small
 291 effective perimeters to become ‘drowned’. However, the effect is relatively subtle and
 292 in some cases the difference in R^2 values is negligible even between designs with large
 293 or small effective perimeter values (e.g., grate types A and H).

294 **Table 3** | Values of experimentally calibrated weir and orifice coefficients (C_w and C_o)
 295 and correspondent goodness of fit R^2 values

Grate	C_w	R^2	C_o	R^2
A	0.115	0.984	0.448	0.987
B	0.208	0.951	1.546	0.974
C	0.194	0.985	0.657	0.991
D	0.115	0.957	0.552	0.950
E	0.135	0.995	0.606	0.998
F	0.204	0.981	1.115	0.994
G	0.157	0.995	1.222	0.976
H	0.372	0.966	2.038	0.967
I	0.264	0.989	0.969	0.989
J	0.168	0.969	0.349	0.978



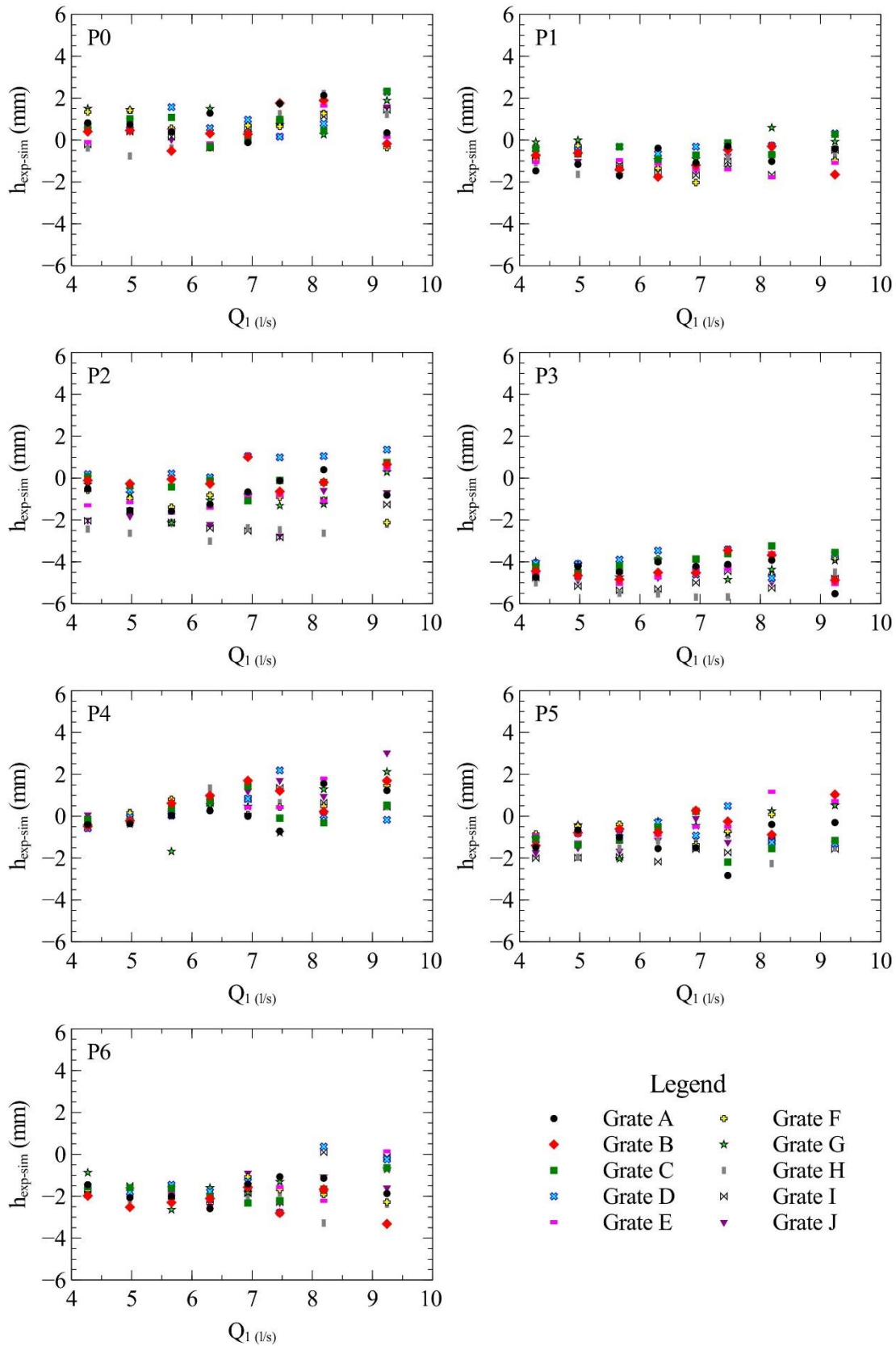
297

298 **Figure 7** | Relationships between experimentally calibrated weir (C_w) and orifice (C_o)
 299 coefficients and geometrical parameters for each inlet grate.

300 **Numerical results**

301 Figure 8 displays the difference between the experimental depths, as measured by the
 302 transducers (Figure 2), with the depths calculated by the numerical model at each
 303 measurement location ($h_{exp} - h_{sim}$). In most locations the numerical results overestimate
 304 the experimentally observed water depths. At locations P_0 and P_4 (i.e., 75 mm left and
 305 right of the inlet), this condition is reversed and the model tends to underestimate
 306 observed water depths. Despite this, overall, the numerical model provides a good
 307 representation of the experimental observations within the range of 0–5 mm of the
 308 experimental values when considering the full range of inlet flow conditions (Q_1).
 309 Modelling errors may be due to the uncertainties related to: (i) the replication of grates
 310 and the correspondent discretisation of the meshing system adopted; (ii) discrepancies
 311 in the floodplain bed elevation applied within the model; (iii) minor effects due to any
 312 skewed inflow from the inlet tank in the experimental model; (iv) use of the upstream
 313 water depth to calculate total flow exchange instead of actual hydraulic head at each
 314 exchange cell as well as any discharge coefficient calibration errors; (v) the depth
 315 averaged nature of the model or other simplifications. Errors are generally seen to be
 316 smaller for the range of $Q_1 = [4.2; 7.46]$ l/s. By analysing each measurement location

317 separately, P_2 and P_3 (i.e., just upstream and downstream of the inlet) show the highest
318 discrepancies (up to 5 mm). This may be related to complex flow patterns forming
319 upstream and downstream of the inlet (such as water accumulation and separation and
320 merging of stream flows) that the model may find difficult to fully replicate.
321 Discrepancies (0–3 mm) are also noted within the pressure measurement P_6 located 460
322 mm upstream of the centreline of the inlet. For measurement locations less influenced
323 by the flow entering the inlet, such as P_1 and P_5 , errors are within the range 0–2 mm. In
324 terms of flow exchange rate, the numerical simulations tend to overestimate the average
325 exchange discharge (on average by 0.25 l/s). Flow exchange calculations within
326 modelling tools are sensitive to calculations of relative head within pipe and surface
327 systems (Rubinato et al. 2017a). In this case, flow exchange is calculated using the
328 calibrated weir equation based on the numerical simulation of flow depth upstream of
329 the inlet. Resulting discrepancies in the simulation of hydraulic water depths around the
330 inlet can therefore be seen to propagate to the calculation of flow exchange rate.
331



332

333 **Figure 8** | Comparison between the experimental observations and numerical hydraulic

334 heads at each measurement location.

335 SUMMARY AND CONCLUSIONS

336 This work has explored the experimental and numerical modelling of surface to sewer
337 flow exchange. A physical model, linking a slightly inclined urban floodplain to a sewer
338 system, was used to carry out measurements under steady state flow conditions with the
339 application of ten different circular grates on the top of a surface/sewer linking
340 structure. Eighty steady state experiments were conducted, during which water levels at
341 seven locations surrounding the inlet structure were measured. The results have
342 confirmed the validity of both the weir and orifice linking equations to describe the total
343 surface to sewer exchange flows through different inlet grates. Calibrated discharge
344 coefficients have been provided for each grate type tested which were taken as constant
345 over the range of hydraulic conditions tested. Overall, the calibrated orifice discharge
346 coefficient showed a larger variation between the grate types. Whilst some evidence
347 was provided to suggest that the weir equation outperforms the orifice equation when
348 the effective perimeter of the grate is relatively high, and vice versa, no significant
349 difference in performance was observed over the range of flow rates tested. Overall
350 trends suggested that discharge coefficients (i.e. energy losses) decrease as the grate
351 geometrical parameters (void area and effective perimeter) increase and may converge
352 to an approximately constant value. In addition, a finite difference numerical model was
353 tailored to reproduce flow conditions around the inlet structure. Experimentally
354 calibrated exchange equations were used to define the inflow through each modelled
355 grate type. The numerical results have been compared with the experiments in terms of
356 depth around the inlet at seven sampling points and detailed comparisons show a regular
357 agreement between the numerical and experimental water levels (maximum discrepancy
358 5 mm). It can therefore be concluded that the proposed 2D numerical approach is able
359 to model floodplain-to-sewer interaction and flow conditions in the vicinity of the
360 linking structure reliably, despite the uncertainties generated by the different geometries
361 of the grates applied and any head variations over the inlet structure. Maximum
362 discrepancies were observed immediately upstream and downstream of the inlet
363 structure, likely due to the complex flow patterns generated by the grate types. While it
364 is not currently feasible to use such methods directly within full scale flood simulations
365 (due to the small mesh sizes required), the work demonstrates the academic capability
366 of the modelling technique and validates the model for supplementary studies. It was
367 also noted that minor discrepancies in the calculation of flow depth propagated to the

368 estimation of flow exchange by the numerical model. Further, more detailed
369 investigation of the exchange flows and the development of modelling approaches that
370 can inherently account for spatially variable energy losses, flow depths and flow
371 exchange rates within different inlet configurations will require characterisation of the
372 velocity fields such that a full understanding of the flow can be elucidated.

373

374 **ACKNOWLEDGEMENT**

375 This research was funded by EPSRC through a grant with the reference EP/K040405/1.
376 The experiments were conducted in the Water Laboratory of the Civil and Structural
377 Engineering Department of the University of Sheffield. Dr. Lee acknowledges the
378 support from the APEC Climate Center.

379

380 **REFERENCES**

- 381 Almedeij, A. O. & Houghtalen, R. J. 2005 *Urban Hydrology: Hydraulics and Storm*
382 *Water Quality*. John Wiley & Son, Hoboken, NJ.
- 383 Bazin, P. H., Nakagawa, H., Kawaike, K., Paquier, A. & Mignot, E. 2014 Modeling
384 flow exchanges between a street and an underground drainage pipe during urban
385 floods. *Journal of Hydraulic Engineering* 140 (10), 04014051.
- 386 Chen, A., Djordjevic', S., Leandro, J. & Savic', D. 2007 The urban inundation model
387 with bidirectional flow interaction between 2D overland surface and 1D sewer
388 networks. In: *NOVATECH 2007 – Sixth International Conference on Sustainable*
389 *Techniques and Strategies in Urban Water Management*, Lyon, France, pp. 465–
390 472.
- 391 Djordjevic', S., Prodanovic', D., Maksimovic', C., Ivetic', M. & Savic', D. 2005
392 SIPSON-simulation of interaction between pipe flow and surface overland flow in
393 networks. *Water Science and Technology* 52 (5), 275–283.
- 394 Djordjevic', S., Saul, A. J., Tabor, G. R., Blanksby, J., Galambos, I., Sabtu, N. & Sailor,
395 G. 2013 Experimental and numerical investigation of interactions between above
396 and below ground drainage systems. *Water Science and Technology* 67 (3), 535–
397 542.
- 398 Gómez, M. & Russo, B. 2009 Hydraulic efficiency of continuous transverse grates for
399 paved areas. *Journal of Irrigation and Drainage Engineering* 135 (2), 225–230.

400 Gómez, M. & Russo, B. 2011a Methodology to estimate hydraulic efficiency of drain
401 inlets. *Proceedings of the Institution of Civil Engineers* 164 (2), 81–90.

402 Gómez, M., Macchione, F. & Russo, B. 2011b Methodologies to study the surface
403 hydraulic behaviour of urban catchments during storm events. *Water Science and*
404 *Technology* 63 (11), 2666–2673.

405 Gómez, M., Hidalgo, G. & Russo, B. 2013 Experimental campaign to determine grated
406 inlet clogging factors in an urban catchment of Barcelona. *Urban Water Journal* 10
407 (1), 50–61.

408 Guo, J. C. 2000a Design of grate inlets with clogging factor. *Advances in*
409 *Environmental Research* 4, 181–186.

410 Guo, J. C. 2000b Street stormwater conveyance capacity. *Journal of Irrigation and*
411 *Drainage Engineering* 72 (5), 626–630.

412 Haleem, D. A., Kesserwani, G. & Caviedes-Voullième, D. 2015 Haar wavelet-based
413 adaptive finite volume shallow water solver. *Journal of Hydroinformatics* 17 (6),
414 857–873.

415 Hammond, M., Chen, A. S., Djordjevic, S., Butler, D. & Mark, O. 2015 Urban flood
416 impact assessment: a state-of-the-art review. *Urban Water Journal* 12 (1), 14–29.

417 Larson, C. L. 1947 Investigation of Flow Through Standard and Experimental Grate
418 Inlets for Street Gutters, Project Report, St. Antony Falls Hydraulic Laboratory,
419 University of Minnesota.

420 Leandro, J., Chen, A., Djordjevic, S. & Savic, D. 2009 Comparison of 1D/1D and
421 1D/2D coupled (sewer/surface) hydraulic models for urban flood simulation.
422 *Journal of Hydraulic Engineering* 135, 495–504. [http://dx.doi.org/10.1061/\(ASCE\)](http://dx.doi.org/10.1061/(ASCE)HY.1943-7900.0000037#sthash.1QracRZb.dpuf)
423 [HY.1943-7900.0000037#sthash.1QracRZb.dpuf](http://dx.doi.org/10.1061/(ASCE)HY.1943-7900.0000037#sthash.1QracRZb.dpuf).

424 Leandro, J., Lopes, P., Carvalho, R., Pascoa, P., Martins, R. & Romagnoli, M. 2014
425 Numerical and experimental characterization of the 2D vertical average-velocity
426 plane at the centre-profile and qualitative air entrainment inside a gully for drainage
427 and reverse flow. *Journal Computer & Fluids* 102, 52–61.

428 Lee, S., Nakagawa, H., Kawaike, K. & Zhang, H. 2013 Experimental validation of
429 interaction model at storm drain for development of integrated urban inundation
430 model. *Journal of Japan Society of Civil Engineers, Ser. B1 (Hydraulic*
431 *Engineering)* 69 (4), 109–114.

432 Lee, S. 2013 Study on Development of Integrated Urban Inundation Model
433 Incorporating Drainage Systems. Ph.D Thesis, Kyoto University.

- 434 Li, W. H., Geyer, J. C. & Benton, G. S. 1951 Hydraulic behaviour of stormwater inlets:
435 I. Flow into gutter inlets in straight gutter without depression. *Sewage and*
436 *Industrial Wastes* 23 (1), 34–46.
- 437 Li, W. H., Goodel, B. C. & Geyer, J. C. 1954 Hydraulic behavior of stormwater inlets:
438 IV. Flow into depressed combination inlets. *Sewage and Industrial Wastes* 26 (8),
439 967–975.
- 440 Lopes, P., Leandro, J., Carvalho, R. F., Páscoa, P. & Martins, R. 2015 Numerical and
441 experimental investigation of a gully under surcharge conditions. *Urban Water*
442 *Journal* 12, 468–476.
- 443 Martins, R., Leandro, J. & Carvalho, R. F. 2014 Characterization of the hydraulic
444 performance of a gully under drainage conditions. *Water Science and Technology*
445 69 (12), 2423–2430.
- 446 Martins, R., Kesserwani, J., Rubinato, M., Lee, S., Leandro, J., Djordjevic´, S. &
447 Shucksmith, J. 2017a Validation of 2D shock capturing flood models around a
448 surcharging manhole. *Urban Water Journal* 14 (9), 892–899. [http://dx.doi.org/10.](http://dx.doi.org/10.1080/1573062X.2017.1279193)
449 [1080/1573062X.2017.1279193](http://dx.doi.org/10.1080/1573062X.2017.1279193).
- 450 Martins, R., Leandro, J., Chen, A. & Djordjevic´, S. 2017b A comparison of three dual
451 drainage models: shallow water vs local inertia vs diffusive wave. *Journal of*
452 *Hydroinformatics* 19 (1). doi:10.2166/hydro.2017.075.
- 453 Rubinato, M. 2015 Physical Scale Modelling of Urban Flood Systems. Ph.D Thesis,
454 University of Sheffield, <http://etheses.whiterose.ac.uk/9270/>.
- 455 Rubinato, M., Seungsoo, L., Kesserwani, G. & Shucksmith, J. 2016 Experimental and
456 numerical investigation of water depths around a manhole under drainage
457 conditions. In: 12th International Conference on Hydroinformatics-Smart Water for
458 the Future, 21–26 August, Songdo Convensia, Incheon, South Korea.
- 459 Rubinato, M., Martins, R., Kesserwani, J., Leandro, J., Djordjevic´, S. & Shucksmith, J.
460 2017a Experimental calibration and validation of sewer/surface flow exchange
461 equations in steady and unsteady flow conditions. *Journal of Hydrology* 552, 421–
462 432. <https://doi.org/10.1016/j.jhydrol.2017.06.024>.
- 463 Rubinato, M., Martins, R., Kesserwani, G., Leandro, J., Djordjevic, S. & Shucksmith, J.
464 2017b Experimental investigation of the influence of manhole grates on drainage
465 flows in urban flooding conditions. In: 14th IWA/IAHR International Conference
466 on Urban Drainage, 10–15 September, Prague, Czech Republic.

- 467 Ten Veldhuis, J. A. E. & Clemens, F. H. L. R. 2010 Flood risk modelling based on
468 tangible and intangible urban flood damage quantification. *Water Science and*
469 *Technology* 62 (1), 189–195.
- 470 Wang, Y., Liang, Q., Kesserwani, G. & Hall, J. W. 2011 A 2D shallow flow model for
471 practical dam-break simulations. *Journal of Hydraulic Research* 49 (3), 307–316.
- 472 Xia, X., Liang, Q., Ming, X. & Hou, J. 2017 An efficient and stable hydrodynamic
473 model with novel source term discretisation schemes for overland flow and flood
474 simulations. *Water Resources Research* 53. doi:10.1002/2016WR020055.
- 475